Comparison of corrosion behavior of primary/modified nickel slag with semi-rebonded periclase-chromite refractory

(Yuchi Liu[1], Hongfeng Yin[1], Songxiong Ding[2], Hudie Yuan[1])

1. Xi 'an University of Architecture and Technology
2. Agder University college

Reporter: Yuchi Liu

E-mail: liuyuchi@xauat.edu.cn

CONTENTS

Background

Nickel sulfide ore

Oxygen-rich top blow smelting

$$2NiS + 3O_2 \rightarrow 2NiO + 2SO_2 \quad (1)$$

$$FeS + NiO \rightarrow NiS + FeO \quad (2)$$

$$NiS + O_2 \rightarrow Ni + SO_2 \quad (3)$$

$$NiS + 2NiO \rightarrow 3Ni + SO_2 \quad (4)$$

（1） Oxidation roasting
（2） Sulfur smelting
（3） Direct smelting
（4） Blowing of sulfur

Nickel

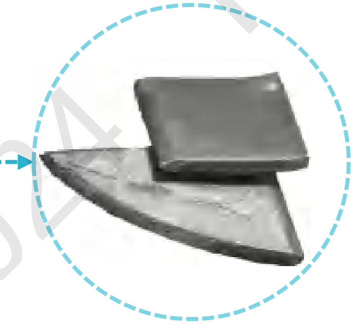

- Stainless steel
- Alloy steel
- Special steel
- Nickel-based alloy
- Electroplate
- Non-alloy area

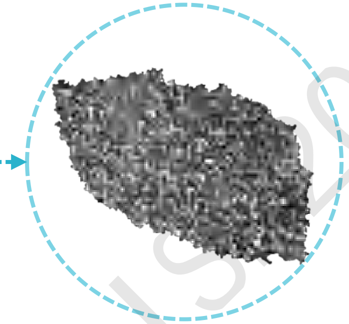

What about this?

Nickel slag

Background

Resources

Reduction

Harmless

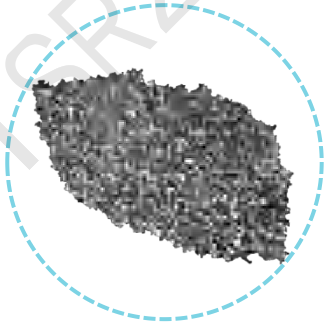

Nickel slag
（TFe 30~45%）

Can be used as a new type of “iron ore resource”

Modifier

$FeSiO_3 \longrightarrow MgFe_2O_4$

From "End Management" to "Process Control"

Idea of extracting iron

Modified Nickel slag

Influence on corrosion resistance of refractories

Part 02

Preparation

Preparation

Table 1 Composition of primary and modified nickel slag (Wt %)

	TFe_2O_3	SiO_2	MgO	CaO	Al_2O_3	Na_2O	K_2O	Ni	Cu
Primary	35.36	47.26	3.50	3.02	1.86	0.46	0.20	4.60	1.47
Modified	33.28	37.52	6.05	15.44	4.05	1.16	0.31	1.23	0.96

Table 2 Properties of the used semi-rebonded periclase-chromite bricks (Wt %)

MgO / %	**Cr_2O_3 / %**	**SiO_2 / %**	**Apparent porosity / %**	**Compressive strength / MPa**	**Refractoriness under load (0.2 MPa, $T_{0.6}$) / °C**
≥58.0	≥18.0	≤2.0	≤16.0	≥40.0	≥1700

Preparation

Table 3 Corrosion conditions and specimen descriptions

Specimens	Temperature/ °C	Time/ h	Slag types
S- P3	1370	3	P
S-P7	1370	7	P
S-P11	1370	11	P
S-M3	1370	3	M
S-M7	1370	7	M
S-M11	1370	11	M

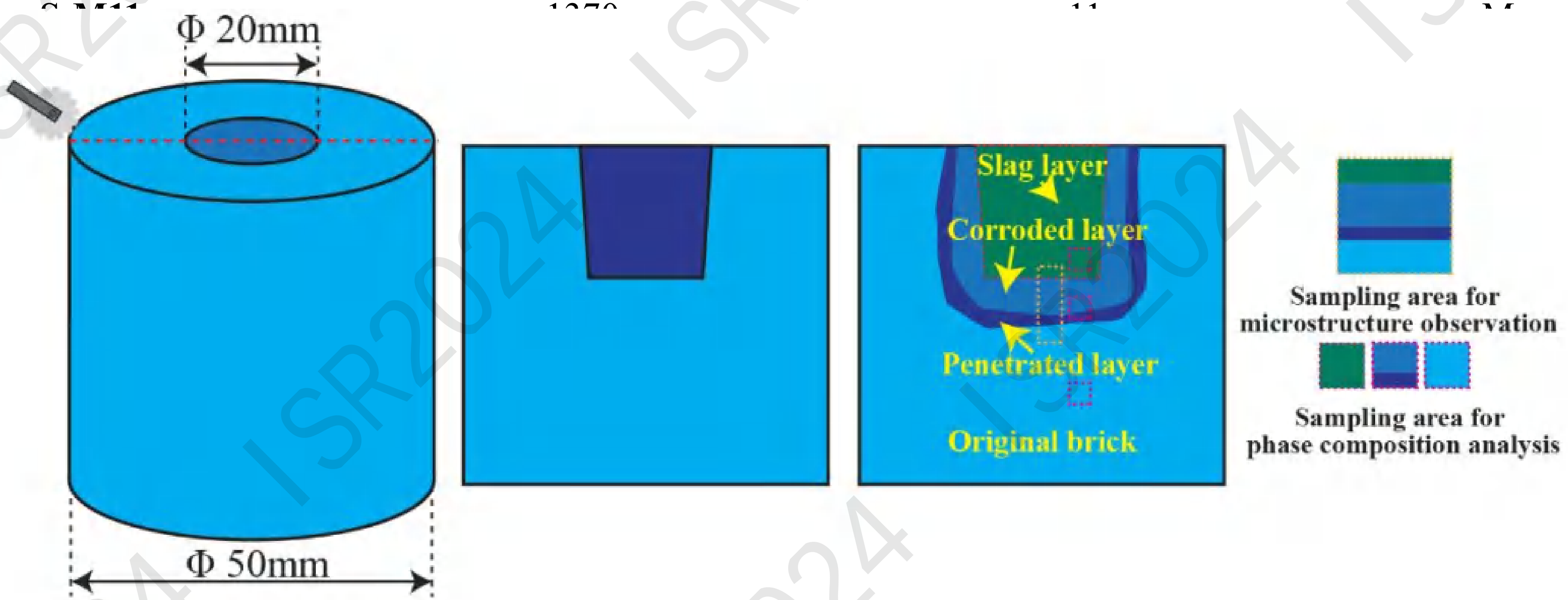

Part 03 Results and discussion

Results and discussion

Diffraction analysis results of raw materials

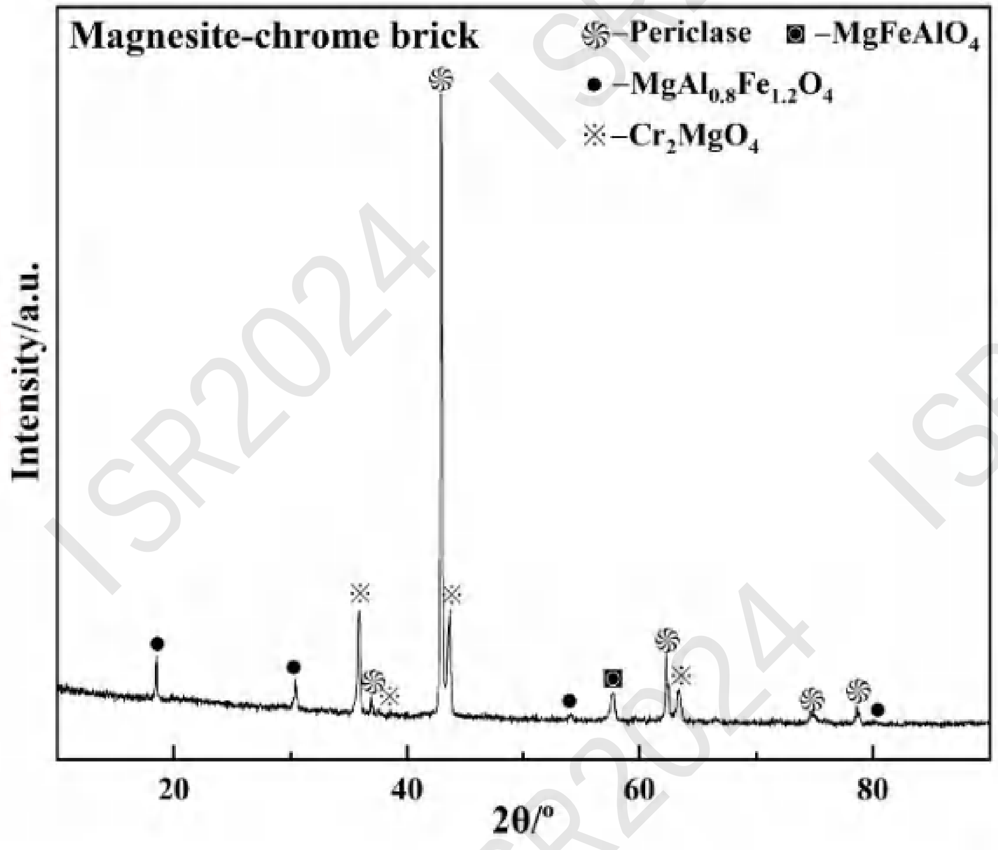

(a) Semi-rebonded periclase-chromite brick

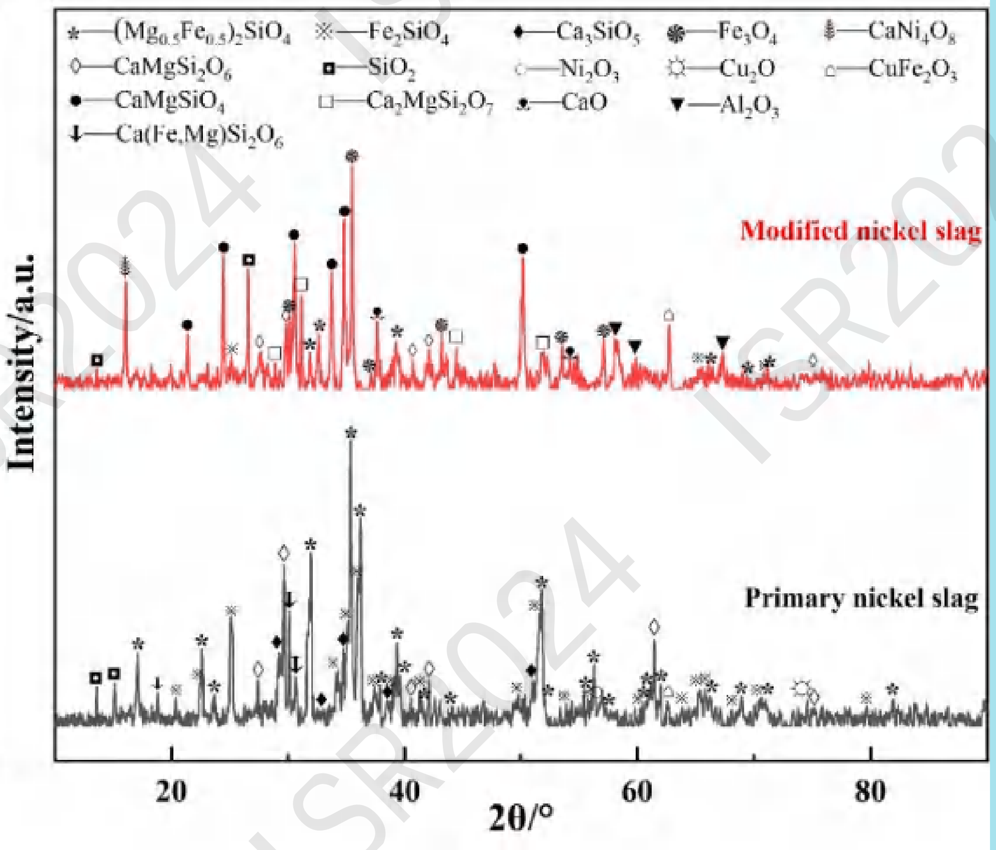

(b) Modified/primary slag

Results and discussion

Diffraction analysis results of corroded samples

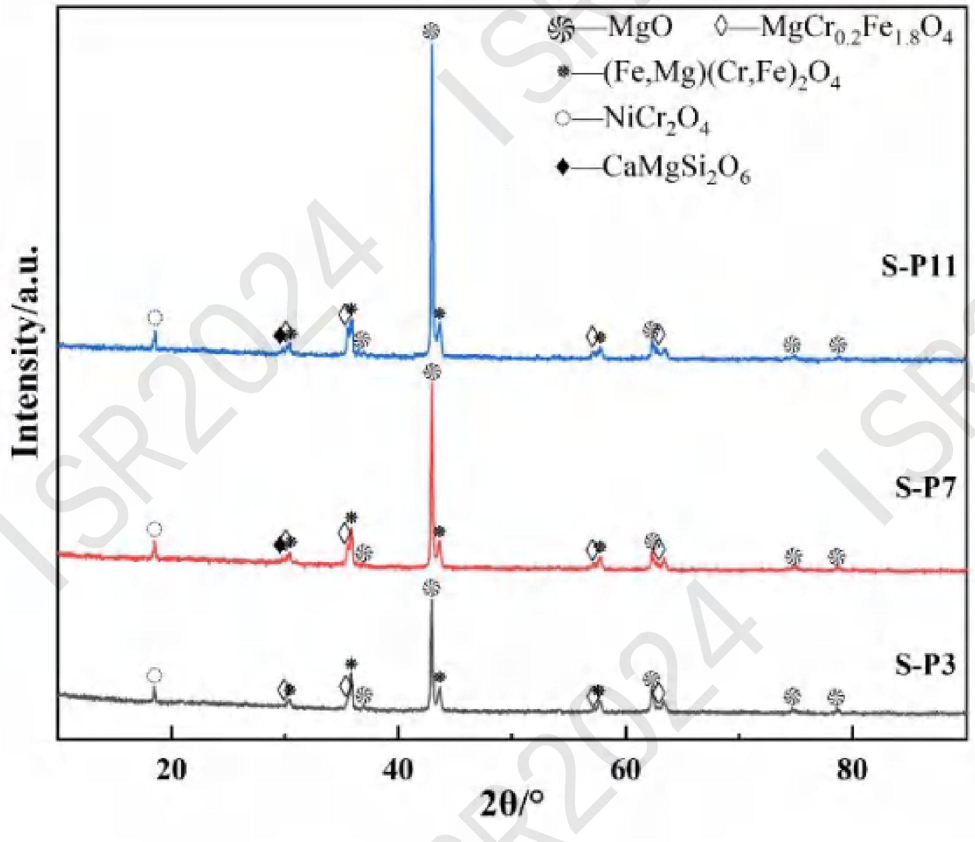

(a) Corroded by primary slag

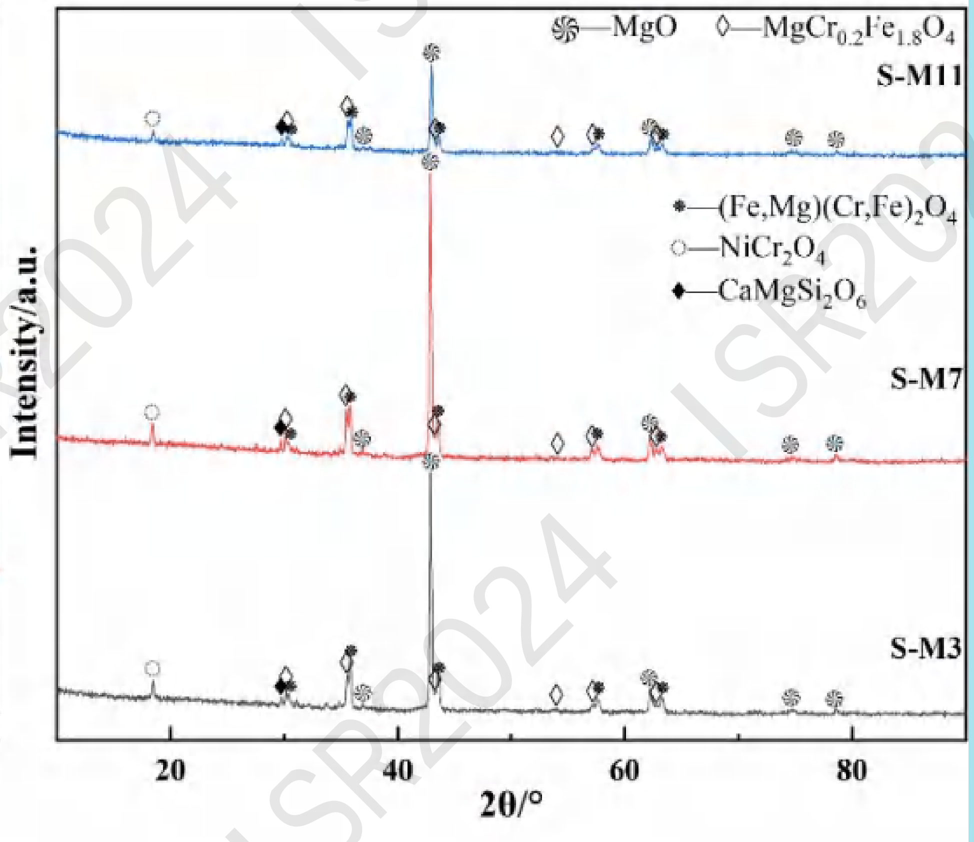

(b) Corroded by modified slag

Results and discussion

Pictures of samples corroded by primary/modified sag

Results and discussion

Microstructure and energy spectrum analysis results of S-P7

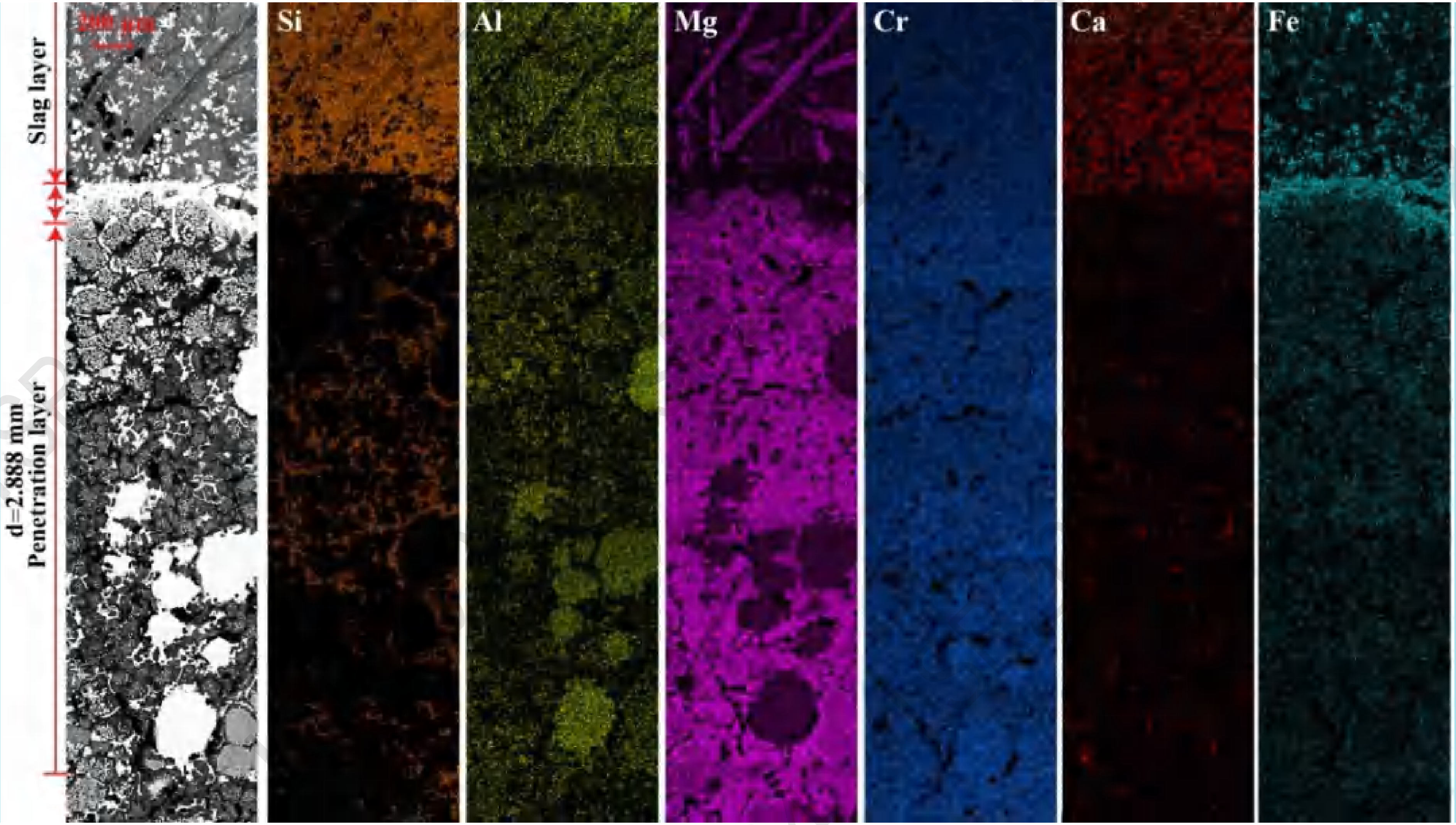

Results and discussion

Microstructure and energy spectrum analysis results of S-M7

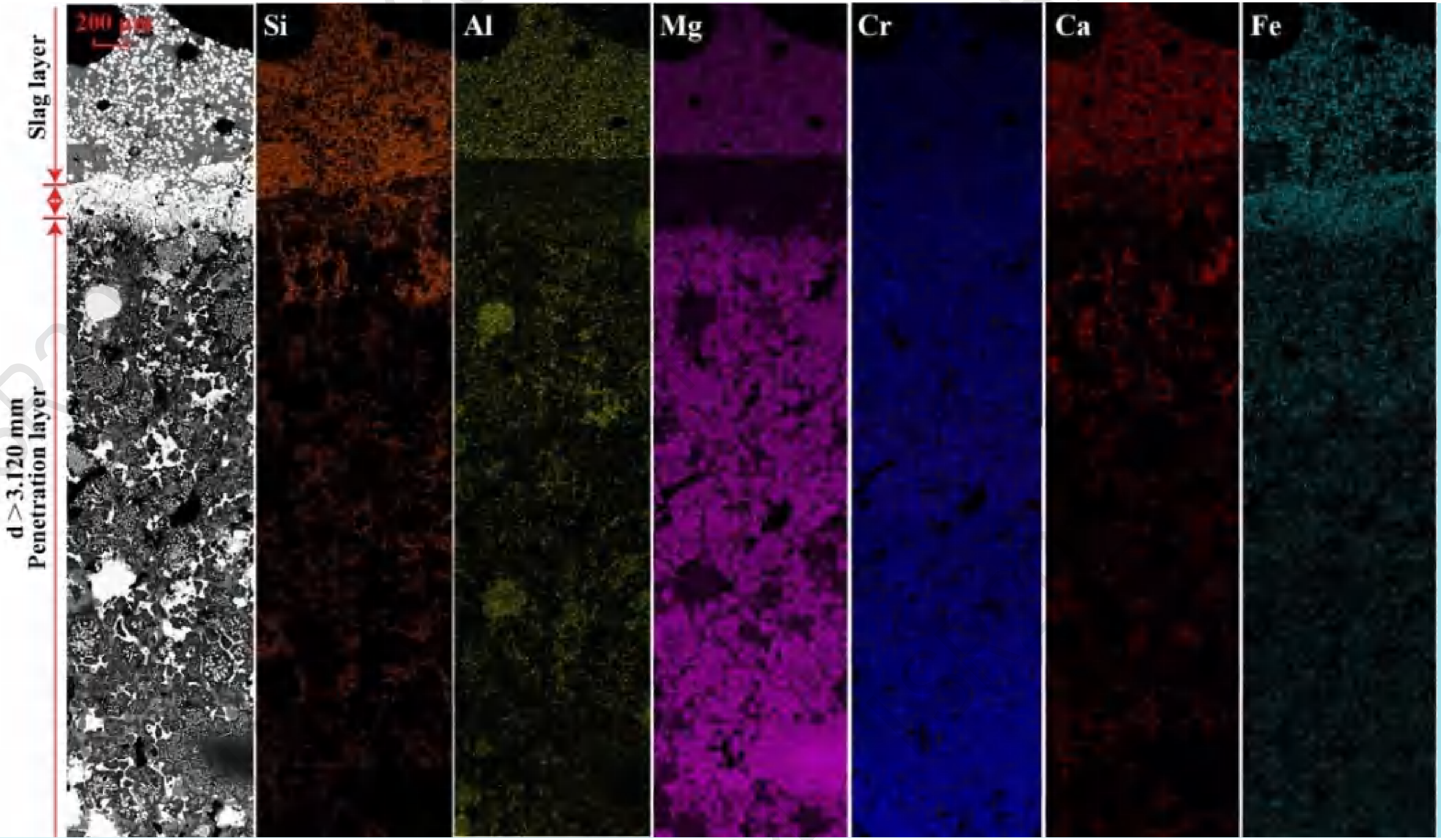

Results and discussion

Microstructure (BSD) of the corroded specimen slag layer (a: S-P3, b: S-M3)

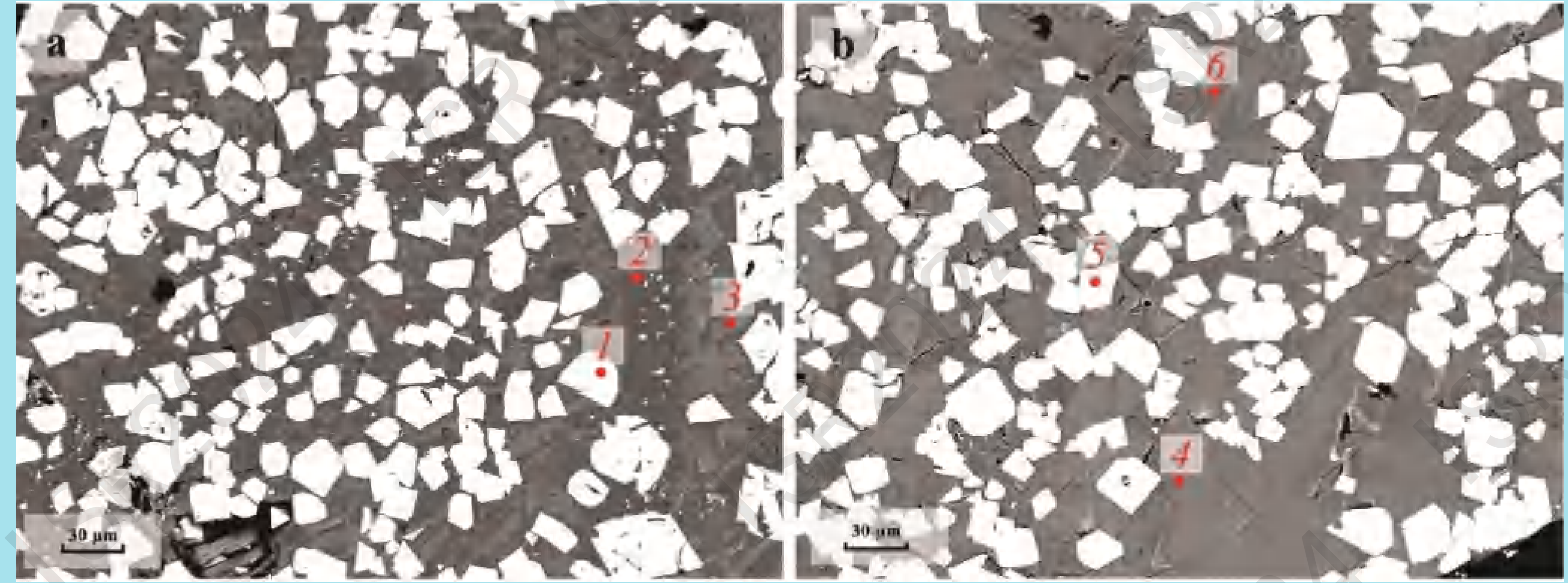

	O	Mg	Al	Si	Ca	Cr	Fe	Ni	Cu
1	29.2	4.0	0.9	2.1	0.3		58.9	4.6	
2	40.5	28.2		19.9	0.3		7.8	3.3	
3	41.5	10.5	0.9	23.7	12.6		10.8		
4	31.7	7.0	2.1	18.6	14.1	11.4	15.1		
5	21.7	6.9	1.5		0.3	13.1	51.7	3.8	1.0

Energy spectrum analysis results for the points

Results and discussion

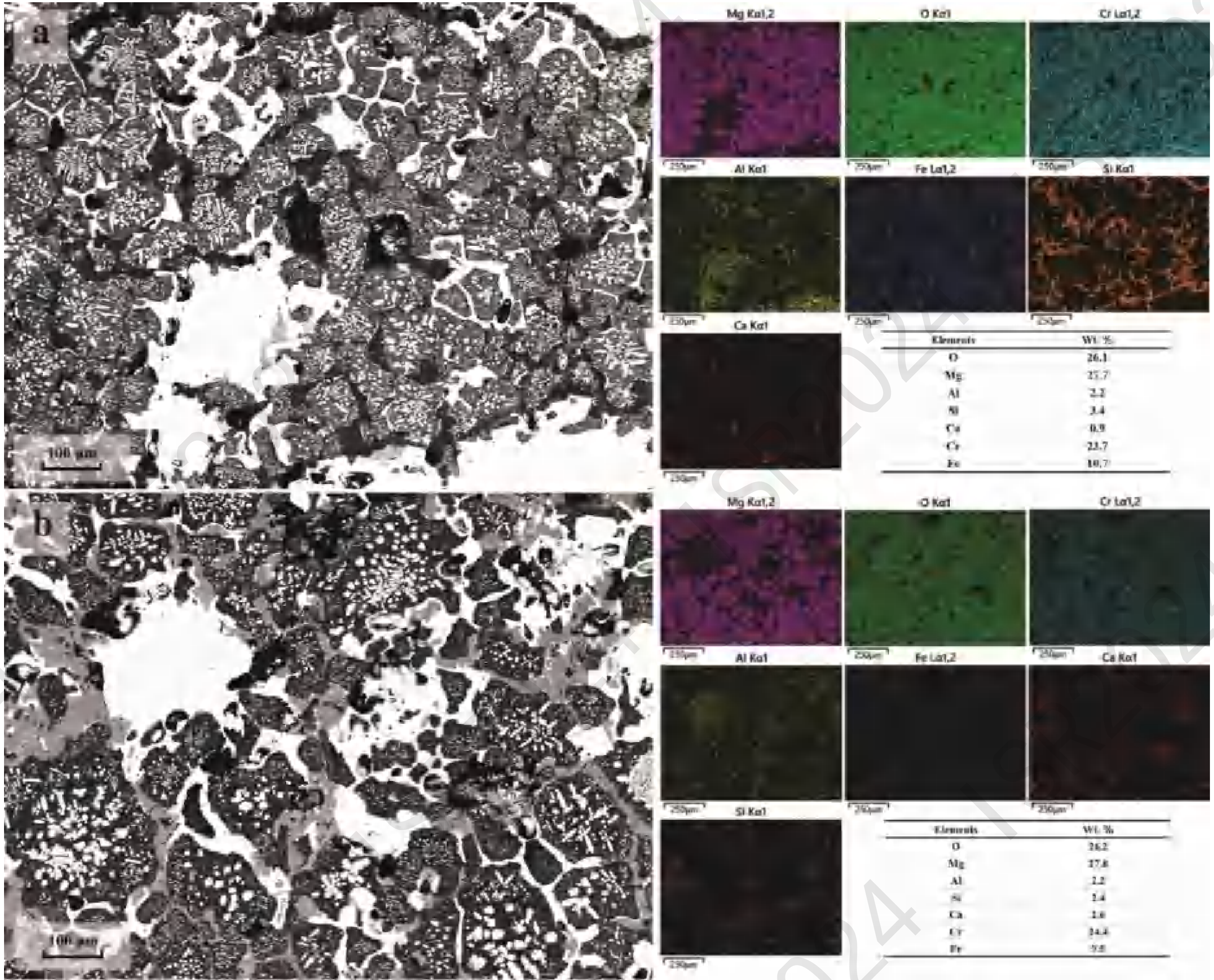

Elements	Wt. %
O	26.1
Mg	25.7
Al	2.2
Si	3.4
Ca	0.9
Cr	23.7
Fe	10.7

Elements	Wt. %
O	26.2
Mg	27.8
Al	2.2
Si	2.4
Ca	2.6
Cr	24.4
Fe	9.8

S-P7

Microstructure (BSD) of the corroded specimen penetration layer

S-M7

Results and discussion

Microstructure (BSD) of the corroded specimen penetration layer (a: S-M11, b: enlarged image for a)

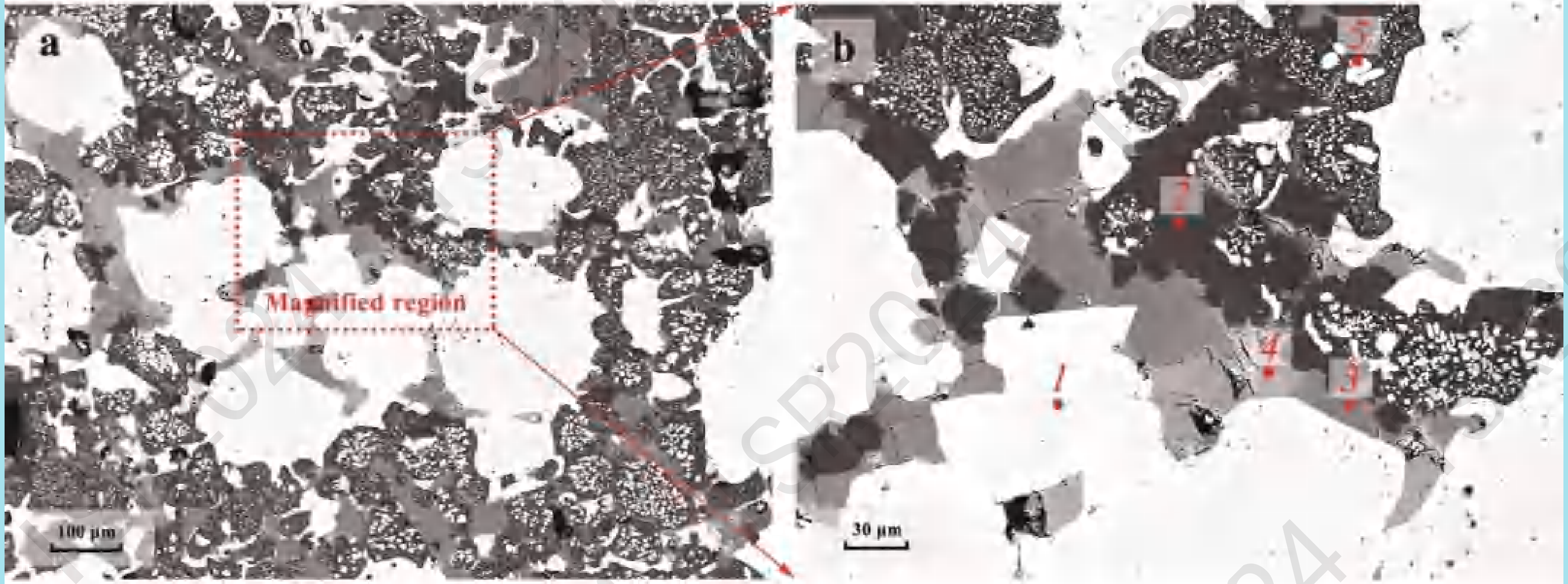

	O	Mg	Al	Si	Ca	Cr	Fe
1	27.1	13.4	8.7			41.0	9.8
2	42.5	33.6		20.9	3.1		
3	41.6	18.7		18.5	21.1		
4	33.3	6.4	5.1	17.3	14.5	9.6	13.9
5	24.9	12.4	6.3			32.3	24.1

Energy spectrum analysis results for the points

Results and discussion

Microstructure (BSD) of the corroded specimen isolation layer (a: S-P3, b: S-M3)

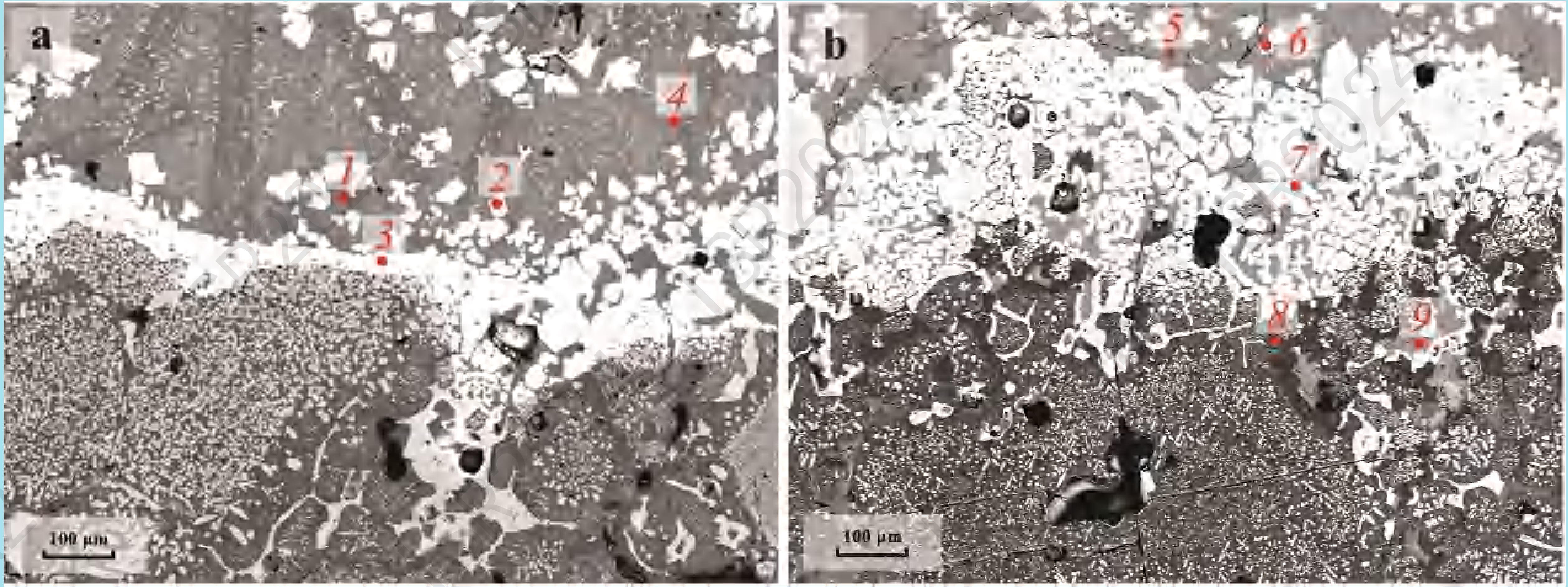

Results and discussion

Energy spectrum analysis results for the points in isolation layer

	O	Mg	Al	Si	Ca	Cr	Fe	Ni	Cu
1	40.7	28.9		18.0			8.8	3.6	
2	19.5	3.0	0.9		0.3	14.9	45.6	5.1	10.7
3	22.3	4.8	1.0			18.1	48.5	5.3	
4	41.4	10.8	0.8	23.8	12.4		10.8		
5	33.3	7.4	2.1	19.1	14.6	9.9	13.6		
6	21.9	7.6	1.6			13.2	51.0	3.4	1.4
7	21.7	9.1	2.0			24.8	40.8	1.8	
8	41.5	33.7		21.0	2.5		1.3		
9	32.3	7.4	2.3	20.0	24.2	11.4	2.4		

Results and discussion

Components of the simulation system

C/S	R	TFe_2O_3	SiO_2	MgO	CaO	Al_2O_3	Na_2O	K_2O	Ni	Cu
0.064	0.44	35.36	47.26	3.50	3.02	1.86	0.46	0.20	4.60	1.47
0.200	0.52	35.36	47.26	3.50	9.45	1.86	0.46	0.20	4.60	1.47
0.400	0.62	35.36	47.26	3.50	18.90	1.86	0.46	0.20	4.60	1.47
0.600	0.73	35.36	47.26	3.50	28.36	1.86	0.46	0.20	4.60	1.47
0.800	0.84	35.36	47.26	3.50	37.81	1.86	0.46	0.20	4.60	1.47
1.000	0.94	35.36	47.26	3.50	47.26	1.86	0.46	0.20	4.60	1.47
1.200	0.99	35.36	47.26	3.50	56.71	1.86	0.46	0.20	4.60	1.47

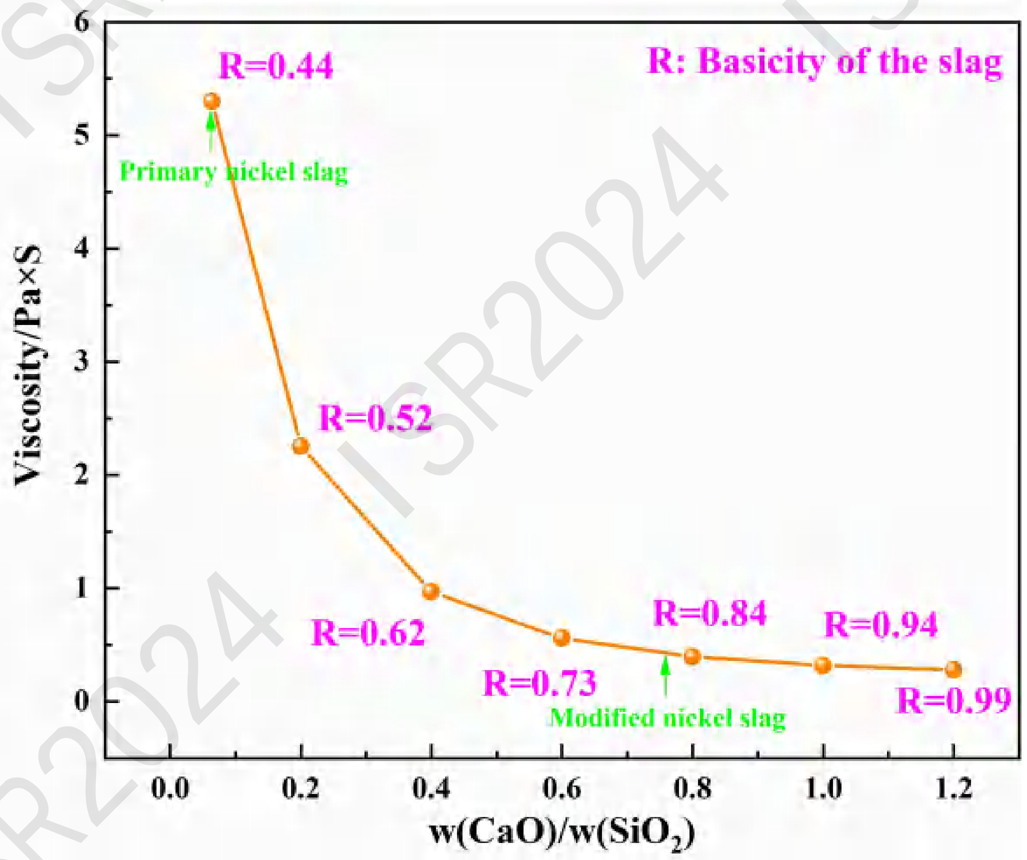

Viscosity of the simulation system at 1370 °C

Results and discussion

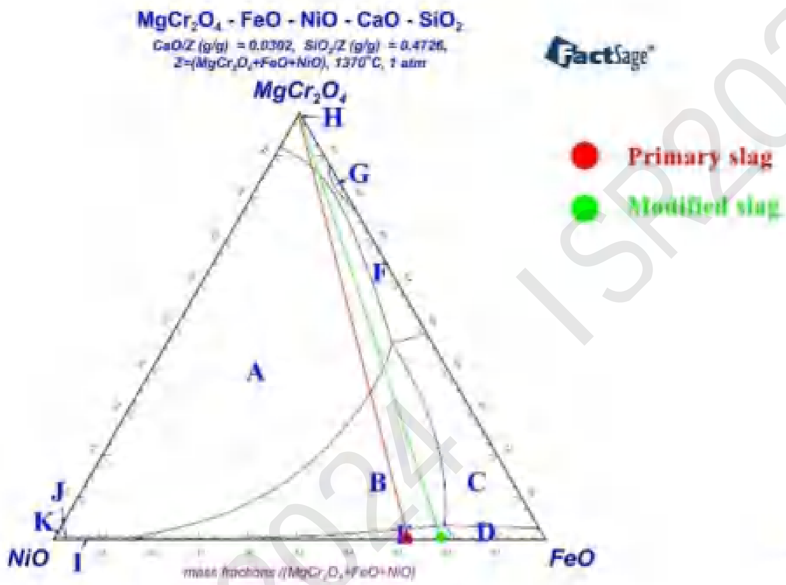

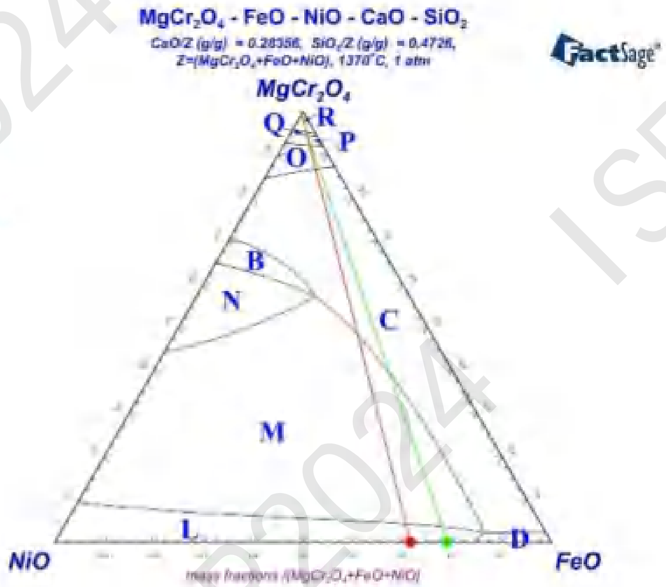

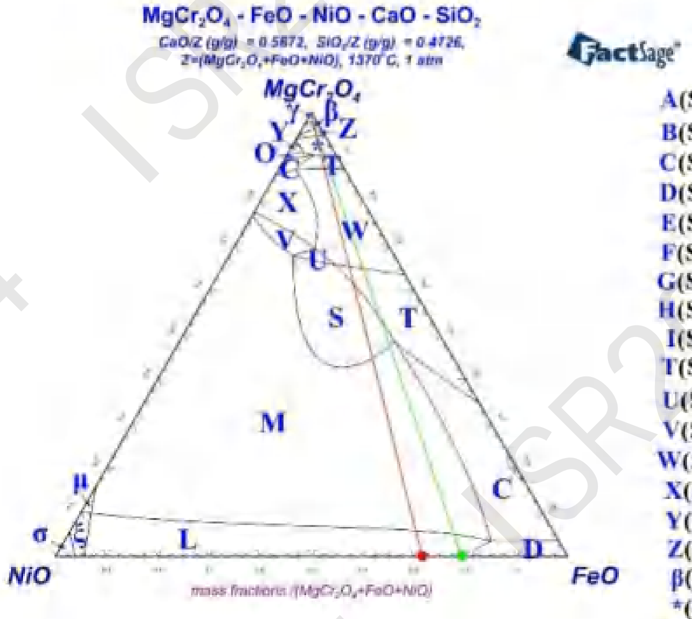

A(Slag+Spienl+Olivine+SiO_2)
B(Slag+Spienl+Olivine)
C(Slag+Spienl)
D(Slag)
E(Slag+Olivine)
F(Slag+Spinel+SiO_2)
G(Slag+Spinel+Clinopyroxene+SiO_2)
H(Slag+Spinel+Cr_2O_3+SiO_2)
I(Slag+Olivine+SiO_2)
T(Slag+Spinel+Ca_2SiO_4)
U(Slag+Spinel+NiO+Ca_2SiO_4+$Ca_3Cr_2Si_3O_{12}$)
V(Slag+Spinel+NiO+$Ca_3Cr_2Si_3O_{12}$)
W(Slag+Spinel+Ca_2SiO_4+$Ca_3MgSi_2O_8$)
X(Slag+Spinel+$Ca_3MgSi_2O_8$)
Y(Slag+Spinel+$CaSiO_3$+$Ca_3Si_2O_7$)
Z(Slag+Spinel+$CaSiO_3$+Ca_2SiO_4+$Ca_3MgSi_2O_8$)
β(Slag+$CaSiO_3$+Ca_2SiO_4+$Ca_3MgSi_2O_8$)
*(Slag+Spinel+$CaSiO_3$+Ca_2SiO_4)

J(Slag+Spinel+NiO+Olivine+SiO_2)
K(Slag+NiO+Olivine+SiO_2)
L(Slag+NiO)
M(Slag+Spinel+NiO)
N(Slag+Spinel+Olivine+NiO)
O(Slag+Spinel+$CaSiO_3$)
P(Slag+Spinel+$CaSiO_3$+$Ca_3Cr_2Si_3O_{12}$)
Q(Slag+Spinel+$Ca_3Cr_2Si_3O_{12}$)
R(Slag+Spinel+Cr_2O_3+$Ca_3Cr_2Si_3O_{12}$)
S(Slag+Spinel+NiO+Ca_2SiO_4)
μ(Slag+Spinel+NiO+$CaSiO_3$)
ξ(Slag+NiO+$CaSiO_3$)
γ(Spinel+Ca_2SiO_4+$CaSiO_3$+$Ca_3Si_2O_7$)
σ(Slag+NiO+$CaSiO_3$+$Ca_3Si_2O_7$)

$MgCr_2O_4$,
Ca_2SiO_4,
$CaSiO_3$,
$Ca_3Si_2O_7$,
$Ca_3Cr_2Si_3O_{12}$,
$Ca_3MgSi_2O_8$

$MgCr_2O_4$-FeO-NiO ternary system under different C/S conditions

Results and discussion

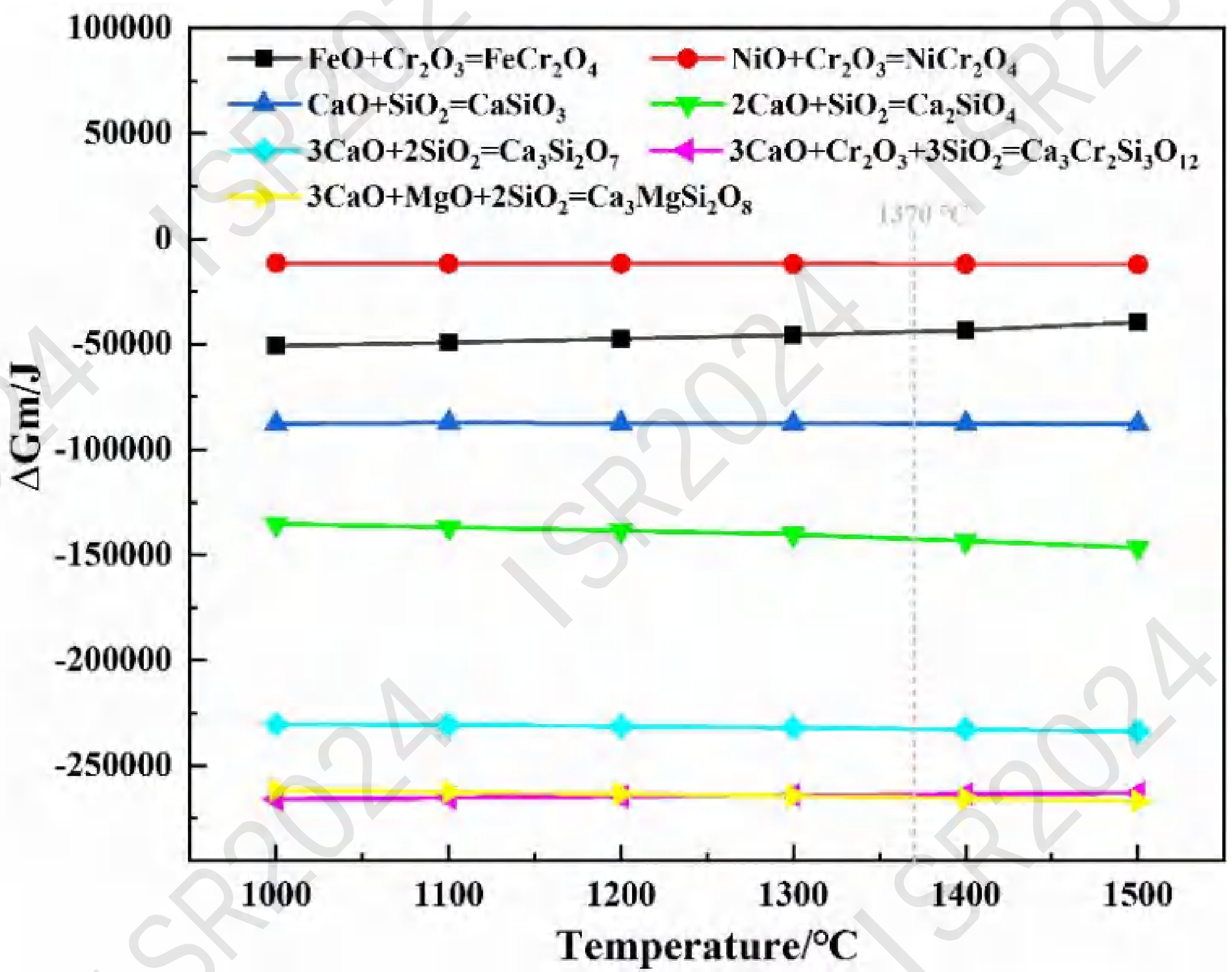

The Gibbs free energy change during the corrosion reaction

$Ca_3Cr_2Si_3O_{12}$ and $Ca_3MgSi_2O_8$

Results and discussion

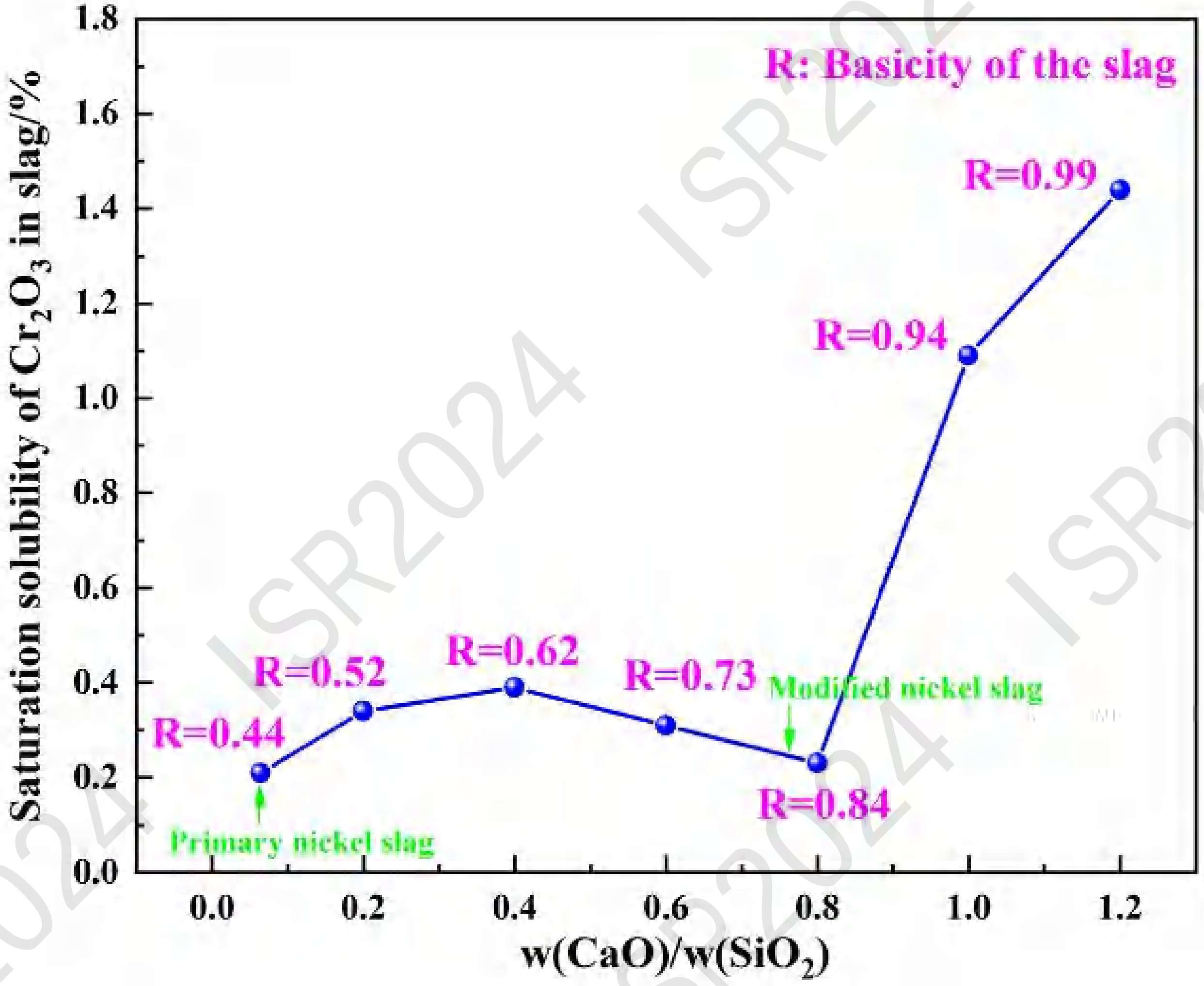

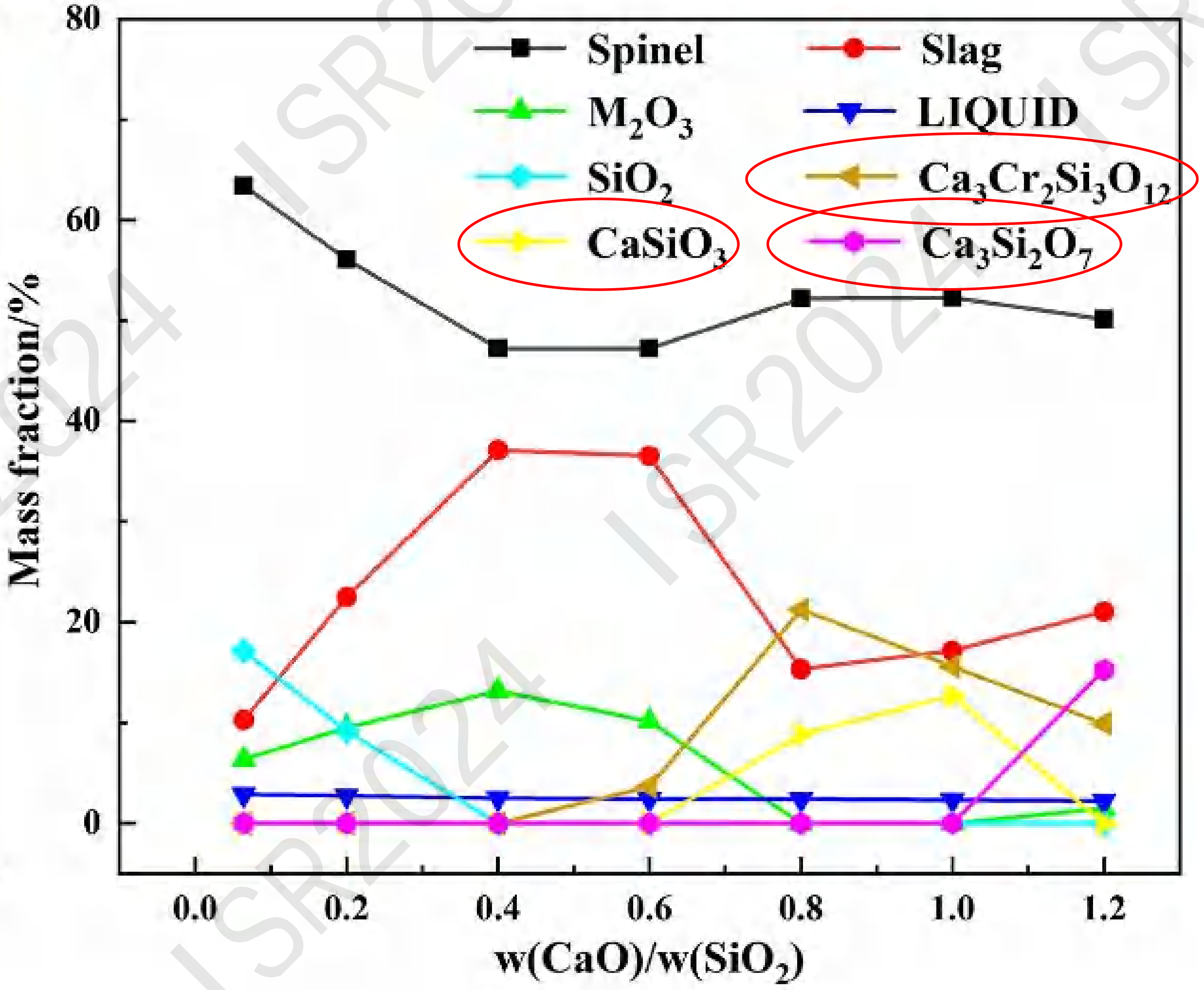

Saturated solubility of Cr_2O_3 in slag and slag composition at different C/S

Results and discussion

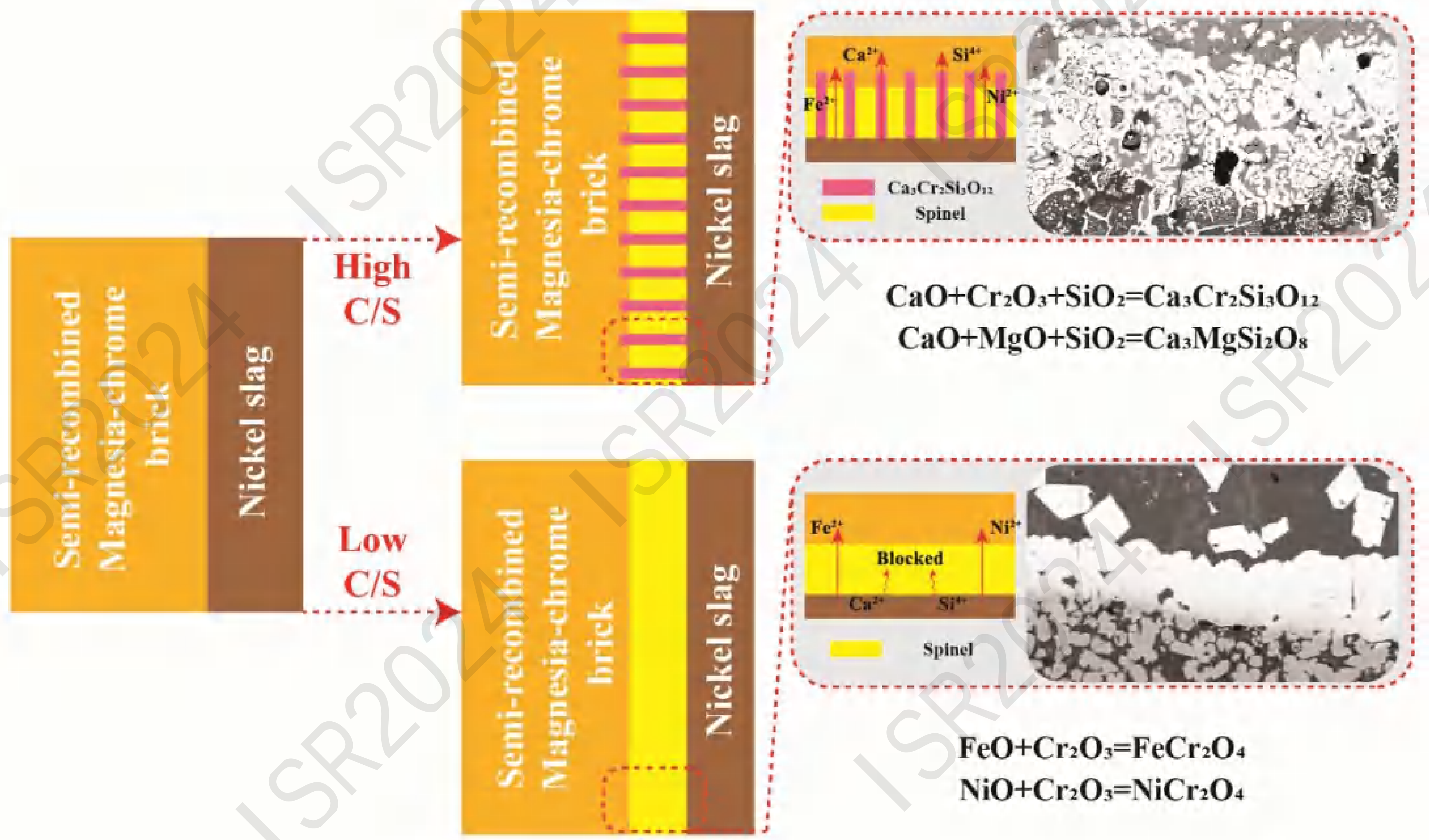

Part 04

Conclusions

Conclusions

The calcium-silicon mass ratio has a substantial influence on the corrosion behavior of semi-rebonded periclase-chromite refractories and nickel slag. A comparative study of the micro-morphology and phase composition of the corroded specimens revealed that the corrosion products emerge largely at the slag-refractory interface. Nickel slag with a high calcium-silicon mass ratio produces corrosion products such as $Ca_3Cr_2Si_3O_{12}$ and $Ca_3MgSi_2O_8$. These chemicals prevent the creation of a continuous isolation layer, allowing Ca^{2+} and Si^{4+} to diffuse through the nickel slag. As a result, nickel slag with a greater calcium-silicon mass ratio is more likely to penetrate the refractory. Semi-rebonded periclase-chromite refractories have a reduced resistance to nickel slag corrosion due to their high calcium-silicon mass ratio.

THANK YOU !